Title

Sample-to-Answer Robotic ELISA

Journal

Analytical Chemistry, 93(33)

ISSN

0003-2700

Authors

Zhou, Chuqing
Fang, Zecong
Zhao, Cunyi
et al.

Publication Date

2021-08-24

DOI

10.1021/acs.analchem.1c01231

Peer reviewed

HHS Public Access

Author manuscript

Anal Chem. Author manuscript; available in PMC 2022 August 24.

Published in final edited form as:

Anal Chem. 2021 August 24; 93(33): 11424–11432. doi:10.1021/acs.analchem.1c01231.

Sample-to-Answer Robotic ELISA

Chuqing Zhou[1,#], **Zecong Fang**[1,2,3,#], **Cunyi Zhao**[4], **Xiyan Mai**[1], **Ameer Y. Taha**[5], **Gang Sun**[4], **Tingrui Pan**[1,2,3,6,7,*]

[1]Micro-Nano Innovations (MiNI) Laboratory, Department of Biomedical Engineering, University of California, Davis, California, 95616, USA

[2]Institute of Biomedical and Health Engineering, Shenzhen Institute of Advanced Technology, Chinese Academy of Sciences, Shenzhen, 518055, China

[3]Shenzhen Engineering Laboratory of Single-molecule Detection and Instrument Development, Shenzhen, 518055, China

[4]Department of Biological and Agricultural Engineering, University of California, Davis, California, 95616, USA

[5]Department of Food Science and Technology, University of California, Davis, California, 95616, USA

[6]Suzhou Institute for Advanced Research, University of Science and Technology of China, Suzhou, 215123, China

[7]Department of Precision Machinery and Precision Instrumentation, University of Science and Technology of China, Hefei, 230026, China

Abstract

Enzyme-linked immunosorbent assays (ELISA), as one of the most used immunoassays, have been conducted ubiquitously in hospitals, research laboratories, etc. However, the conventional ELISA procedure is usually laborious, occupies bulky instruments, consumes lengthy operation time, and relies considerably on the skills of technicians, and such limitations call for innovations to develop a fully automated ELISA platform. In this paper, we have presented a system incorporating a robotic-microfluidic interface (RoMI) and a modular hybrid microfluidic chip that embeds a highly sensitive nanofibrous membrane, referred to as Robotic ELISA, to achieve human-free sample-to-answer ELISA tests in a fully programmable and automated manner. It carries out multiple bioanalytical procedures to replace the manual steps involved in classic ELISA operations, including the pneumatically driven high-precision pipetting, efficient mixing and enrichment enabled by back-and-forth flows, washing, as well as integrated machine vision for colorimetric readout. The Robotic ELISA platform has achieved a low limit of detection (LOD) of 0.1 ng/mL in the detection of a low sample volume (15 μL) of chloramphenicol

[*]**Corresponding Author** Tingrui Pan. Tel.: +086-512-87161133. tingrui@ustc.edu.cn.

[#]C.Z. and Z.F. contributed equally to this work.

Supporting Information

(i) Nanofibrous membrane fabrication, (ii) Layer-by-layer (LBL) assembly of the microfluidic ELISA chip (Figure S1), (iii) Flow resistance of the key segments in the microfluidic ELISA chip (Table S1) and (iv) Demo video (mp4). The Supporting Information is available free of charge on the ACS Publications website.

(CAP) within 20 min without human intervention, which is significantly faster than that of the conventional ELISA procedure. Benefiting from its modular design and automated operations, the Robotic ELISA platform has great potential to be deployed for a broad range of detections in various resource-limited settings or high-risk environments, where human involvement needs to be minimized, while the testing timeliness, consistency and sensitivity are all desired.

INTRODUCTION

Immunoassays, as one of the most commonly used biochemical tests, have been conducted ubiquitously in hospitals, research laboratories, etc.[1] Since its origination in the 1950s, immunoassays have become the most commercially successful diagnostic technology, covering applications from home pregnancy testing to AIDS testing and to the most recent COVID-19 diagnosis, etc.[1,2] It typically relies on a specific and strong interaction between an antibody and an antigen to detect a potential target analyte, which ranges from natural and man-made chemicals, biomolecules, cells to viral particles, etc.[1] Specifically, a classic immunoassay consists of three components, namely an antibody, an analyte (antigen), and a detectable label for the indication and signaling of the antibody-antigen binding events. Thus, the immunoassays can be classified into multiple types according to the various forms of labels, including enzymes, radioactive isotopes, fluorophore, chemiluminescent probes, microbeads, and nanoparticles, etc. Among them, the most popular labels used are enzymatic types, owe to the simple molecular design in the overall assay; and the corresponding enzyme-linked immunosorbent assays (ELISA), therefore, have become the most common immunoassay. Notably, almost all existing diagnostic laboratories may have already encountered at least one form of ELISA tests.[1,3] In its simplest form, the conventional ELISA contains solid-phase reactions between an antibody (Ab) immobilized on a solid-phase platform (e.g., 96 well microtiter plates) and an antigen (Ag) in a liquid sample.[1] Despite its advantages including simplicity in design and high sensitivity in detection, the conventional manually operated ELISA has experienced some major drawbacks. For instance, the assay procedure is usually laborious since it involves multiple liquid pipetting, washing, and incubation steps, in addition to the lengthy reaction time involved.[4] Moreover, it relies considerably on the skills of technicians, making it critical to obtain reproducible and consistent results.[4] Finally, the heavy human involvement requires numerous administrative and regulatory efforts in the procedure to minimize the harms of a target analyte that could be toxic, infectious, and sometimes even fatal to the operators. Such limitations of the conventional ELISA procedure call for innovations to automate the multiple liquid handling and readout steps and eventually eliminate the participation of humans, ideally leading to a fully automated human-free ELISA procedure.[4]

The commercial automation efforts for ELISA operations have been primarily focused on the standard well plate platforms. Some of the representative automated ELISA systems are shown in Table 1. A range of specialized instruments have been designed to fit the microwell plates, such as robotic pipetting devices, washers, shakers, incubators, and microtiter plate readers. More recently, fully automated ELISA systems have been implemented to integrate the aforementioned components into one piece of equipment. Representative commercial products include Freedom EVO® ELISA Biopharma from Tecan, Crocodile ELISA

miniWorkstation from BERTHOLD TECHNOLOGIES, ELISA STARlet from HAMILTON Robotics, and Agility® ELISA from Abbott, etc. Although such systems have enabled the fully automated functions of the ELISA procedure and some of them are capable of processing up to hundreds of samples at a time, they typically possess a large footprint and are expensive to acquire, and thus, are not intended to be used in the research laboratories or resource-limited clinics. Furthermore, these conventional well plate-based platforms have relatively low efficacies of molecular adsorptions and the correspondingly low sensitivity of readouts due to the limited surface-to-volume ratio of the wells.[4]

As an emerging transformative technology, microfluidics has begun to reshape the conventional bioanalytical fields, including ELISA systems, over the past decades, with the potential to offer 1) affordability, 2) sensitivity, 3) specificity, 4) user-friendliness, 5) rapid and robust, 6) equipment-free, and 7) deliverable to those in need for such technologies, as outlined by the World Health Organization (WHO).[4] Table 1 features a group of representative microfluidic-enabled ELISA automation systems. Based on the primary constructive materials, the automated microfluidic ELISA systems could be categorized into polymeric, paper-based, or hybrid devices. Among them, the polymeric ELISA chips employ various mechanisms for liquid handling, including capillary force[6], centrifugal force[8], off-the-chip[7] or integrated pumps and valves[9,12]. For instance, Lee, Cho and their colleagues have designed a fully automated disc-shaped microfluidic ELISA system for the detection of infectious diseases from whole blood, with microbead-based suspensions, in which plasma separation, incubation, washing, and enzyme reaction are incorporated, and an integrated detector module made of photodiodes and LEDs is used for absorbance detection.[8] As manifested in Table 1, such microfluidic ELISA platform miniaturizes the whole system and offers various advantages such as a significantly reduced sample volume (1-50 μL), shorter duration of assays (10-60 minutes), enhanced sensitivity (limit of detection from 0.01 to 0.51 ng/mL), portability and small footprint, when compared to that of a conventional plate-based ELISA.[5] However, such polymeric microfluidic chips naturally require complex fabrication processes such as multilayer photolithography or injection molding. In addition, the surface area of the microchannel is limited to the bindings of proteins. Furthermore, a dedicated readout instrument is typically required with the involvement of costly microparticles for labeling.

Alternatively, the paper-based microfluidic devices have appreciably more surface area available for Ab-Ag binding, benefiting from their intrinsic 3D nanoscopic topology. They are cost-effective, and therefore, can be readily deployed in resource-limited settings.[13] One pioneer work in the automation of paper-based ELISA have been proposed by Chailapakul, Takamura and their colleagues, which has patterned flow barriers on a nitrocellulose (NC) paper for the control of fluid flow and used capillarity for the purely passive automatic loading of the liquid onto the paper, thus eliminating any external dedicated instrument for flow control.[10] Despite of the increased binding sites and the device simplicity, the paper-based ELISA methods have limited sensitivity compared to the polymeric devices, largely due to the restricted hydrodynamic forces under the purely passive capillary-driven flow.[6] Recently, a nanofibrous membrane (NFM)-based ELISA system has been presented, utilizing an extremely high surface-to-volume ratio of NFM for the efficient Ab immobilization, which has been proven with a significantly higher sensitivity than that of

the conventional NC papers.[14] With such efficient immobilization, the NFM-based ELISA device has enabled naked-eye colorimetric detection at a low limit of detection of 0.3 ng/mL, within a rapid incubation window of 5 min.[14] However, the emerging NFM-based ELISA system has yet to be automated, mainly due to the lack of solutions to handle and manipulate the NFM substrates automatically and conveniently.

By combining the features of both the polymeric and the paper-based devices, the hybrid ELISA chip offers additional advantages over its predecessors. In one recent work by Li's group, a reusable PMMA/paper hybrid device has been designed to enable plug-and-play, resulting in high-sensitivity and low-limit detection of immunoglobulin G (IgG) down to 0.2 ng/mL.[5] In particular, a pre-patterned paper is inserted into a simplified PMMA microfluidic device with preset slots, and the sample is then infused into the device to flow back-and-forth through the paper, enabling enhanced analyte enrichment and efficient washing.[5] Although various studies have significantly improved sensitivities and expanded dynamic ranges of hybrid microfluidic devices to the conventional ELISA operations, the current approaches are still far from being fully automated. For instance, an external flow drive (e.g., a syringe pump) is needed to attach to the system, while the microfluidic chip has to be manually placed for scanned readout.

Recently, our group has introduced the first modular robotic-microfluidic interface (RoMI) for the world-to-chip bridging. The fully automated manipulation of the modular microfluidic devices using a standard robotic arm has been implemented with operations such as recognition, capturing, positioning, and liquid handling.[15] In this study, we have extended the RoMI platform for the automation of ELISA, referred to as Robotic ELISA, by incorporating a modular microfluidic chip that embeds the aforementioned ultrasensitive NFM-based biosensor into a layer-by-layer polymeric construct. The fully automated robotic system is intended to carry out multiple bioanalytical procedures to replace all the manual steps involved in classic ELISA operations, including the pneumatically driven high-precision pipetting, mixing, efficient washing, as well as integrated machine vision for colorimetric readout, leading to a facile human-free sample-to-answer workflow of ELISA. Moreover, the microfluidic chip is designed to accommodate a standard modular fabrication procedure and assembled layer-by-layer into an integrated device, which can be captured and released by the robotic effector reversibly. Benefiting from the modular microfluidic design, the automated back-and-forth flows of the liquid samples and subsequent reagents through the NFM sensors have been achieved, and as a result, the Ab-Ag binding efficacy and the overall sensitivity has been significantly improved, relative to that of the manual operations of the same procedure.[14] As a demonstration, we have successfully applied the Robotic ELISA platform to the automated detection of chloramphenicol (CAP), a banned antibiotic in the US. All of the ELISA operations from sample preparation to signal readout have been automatically completed within 20 min without human intervention, of which the reaction volume (15 μL) is an order of magnitude lower than that of the conventional ELISA methods using 96-well plates, and the limit of detection (LOD) achieved is 0.1 ng/mL. Benefiting from its modular design and automated operations, the Robotic ELISA platform could be potentially deployed for a broad range of detections in resource-limited settings or high-risk environments, where human involvement needs to be minimized, while the testing timeliness, consistency and sensitivity are all desired.

OPERATING PRINCIPLES

The Robotic ELISA system is designed to fully automate the entire ELISA workflow via the novel robotic-microfluidic interface (RoMI), which precisely positions the microfluidic chip, reversibly connects the pneumatic drives mounted on the robotic arm to the chip for automated liquid handling, and consecutively enables optical readout, followed by the waste disposal. Specifically, its operations include robotic loading, pipetting, mixing, washing, reaction, incubation, and colorimetric detection. As shown in Fig. 1a, the Robotic ELISA platform comprises three major components, namely the hybrid microfluidic ELISA chip, the robotic arm equipped with a pair of the RoMI effectors that incorporate pneumatic connectors for microfluidic control, and a high-definition vision unit for colorimetric detection.

First, the ELISA chip design has four major segments, that is, a serpentine channel connected to the chip tip for flow regulation, a detection chamber (with the nanofibrous membrane embedded inside), a planar buffer chamber, and a RoMI interconnect, as shown in Fig. 1b. The serpentine channel is connected to the detection chamber, which has an embedded nanofibrous membrane for the solid-liquid reactions, and the detection chamber is connected to the funnel-shaped liquid reservoir. The funnel shape is designed to aid the wetting of the side walls of the buffer chamber and avoid the trapping of air bubbles as it becomes filled with liquid.[16] In the microfluidic model to describe the fluid dynamics, the serpentine channel is designed to have significantly greater flow resistance than the rest. Therefore, during the aspiration of the reagents, the aspiration rate can be precisely controlled, according to the hydraulic Ohm's law under laminar flow conditions, $\Delta p = R_f \cdot Q$, where Δp is the pressure difference applied, Q is the flow rate, and R_f is the flow resistance, a geometrically governed and liquid-specific constant.[17] Accordingly, the aspirated volume can be controlled, by precisely timing the duration of the aspiration using a high-precision solenoid valve that links to the RoMI effectors.

Second, on the robotic arm, the pair of the RoMI effectors are made from custom-designed and 3D-printed adapters to the robotic arm.[15] In particular, one side of the RoMI effector is connected to the pneumatic drive with precisely controlled pressure (either negative or positive) via a solenoid valve, while the other side can reversibly engage to the RoMI interconnect on the ELISA chip, upon gripping and clamping. As a result, the negative or positive pressure from the pneumatic drive can be directly applied to the microfluidic chip upon the gripping of the RoMI effector onto the chip, to perform the control of liquid handling. Third, the vision unit attached to the robotic arm can be used for the real-time colorimetric readout of the nanofibrous membrane inside the detection chamber. The imaging data can then be wirelessly transmitted and analyzed instantaneously.

As a demonstration, Fig. 2 depicts the use of the Robotic ELISA system in a standard competitive ELISA protocol, which includes the operations of high-precision metering, mixing, washing, enzymatic reaction, and robotic-vision enabled imaging and detection. First, the high-precision metering can be achieved through the pneumatically driven aspiration.[17] As mentioned previously, the aspiration rate can be fine-controlled by designing the serpentine channel with high flow resistance, and the aspiration volume

can be adjusted by precise timing of the solenoid valve. Specifically, the process starts with sequential and quantitative aspiration of a sample solution (Fig. 2a) and a target conjugated horseradish peroxidase (target-HRP) solution (Fig. 2b), consecutively. Next, a mixing process can be achieved by alternately applying negative and positive pressure to the buffer chamber, thus aspirating the liquid through the device, similar to that of conventional pipette operations (Fig. 2c). In addition, the solutions can sufficiently mix with the antibody-immobilized nanofibrous membrane inside the detection chamber during the aspiration, as the convective flow increases the chance of contact between the multiple samples and reagents with the membrane.[5] As a result, the number of analytes bound to the antibodies can be increased and the incubation time is shortened.[5] As shown in Fig. 2d, efficient washing can be realized by a similar convective flow of the buffer solution enabled by the alternating pneumatic pressures. Finally, an enzymatic reaction is introduced by robotic loading of the colorimetric reagent of 3,3',5,5'-Tetramethylbenzidine (TMB) into the detection chamber in Fig. 2e. The vision unit on the robot is then used to automatically record the real-time colorimetric change of the membrane, from which a recognition algorithm is applied to quantify the colorimetric results. A demonstration video of the complete Robotic ELISA operations has been included in the ESI, successfully showcasing its fully automated sample-to-answer workflow.

EXPERIMENTAL METHODS

Integration of the Robotic ELISA system

The Robotic ELISA system mainly consists of three control modules: a professional SCARA robot arm (M1, Dobot), a pressure control unit (PG-MFC, PreciGenome), and a valve control unit that contains a valve manifold and high precision solenoid valves (LHDA2421111H, The Lee Company, USA). The system was communicated and controlled by a computer via USB ports in a programmable manner (with Python). Specifically, the robotic arm was programmed to grab, move, and release the hybrid microfluidic chip, with a maximum working range of 400 mm and a rated precision of 0.02 mm; the pressure control unit was programmed to set the pneumatic pressure level in the valve manifold within the range of −7 to 13 psi at a precision of 0.1 psi; the valve control unit was programmed to adjust the opening and closure duration of the solenoid valve with millisecond precision.

A pair of custom 3D printed RoMI effectors were designed to connect the air flow from the valve manifold to the RoMI interconnect on the hybrid microfluidic chip, with incorporated silicone rubber O-rings to ensure tight sealing. They were designed in SolidWorks and fabricated with a Clear Resin (Formlabs) using SLA 3D printer (Formlabs Form 3, USA). The RoMI effector linked the outlet of the valve manifold and the RoMI interconnect on the microfluidic chip. A test bench was set at the center of the robot arm’s working area. A custom microplate adapter was fastened on the test bench and pre-calibrated. The images were captured in a programmable manner using a USB link between the lab PC and a miniature camera (HM1355, Banggood, USA). OpenCV library (Python version 3.7) was used to identify the periphery of the nanofibrous membrane inside the hybrid microfluidic chip and calculate the averaged grayscale value (color intensity) within the membrane.[18,19] Each captured image has more than 2000-pixel effective grayscale values processed. In

addition, the uniformity of the colorimetric readouts on the membrane were evaluated, by calculating the deviation of grayscale values; only those membranes that resulted in a uniform colorimetric distribution with a relative deviation of less than 20% were used in our experiments.

Fabrication of the hybrid microfluidic ELISA chip

The nanofibrous membrane-contained hybrid microfluidic device can be prepared via laser micromachining and repetitive layer-by-layer (LBL) assembly. As illustrated in Fig. S1, the device consists of five layers, including three structural layers made of PMMA sheets (Astra Products) and two layers made of pressure-sensitive adhesive (Adhesives Research, Inc.), and the nanofibrous membrane can be incorporated in the third layer. Specifically, the first layer is 1 mm thick and has a 1 mm opening that serves as the RoMI interconnect; the second layer has a thickness of 48 μm, with a serpentine microfluidic channel incorporated; the third layer has a thickness of 0.5 mm with a detection chamber (2 mm in diameter) for the nanofibrous membrane to reside and a buffer chamber to store the reagents; the fourth layer has a thickness of 48 μm and the fifth layer has a thickness of 1 mm. All the five layers were designed in AutoCAD (Autodesk Inc.) and laser-cut (Universal Laser Systems, VersaLaser 2.30) into the designed pattern. Each of the laser-cut layers was inspected under a microscope (EVOS XL, Life Technologies) and the channel width was measured and analyzed using ImageJ (National Institutes of Health). Finally, the five layers were carefully aligned and assembled layer by layer under an inverted stereoscope.

Characterization of the hybrid microfluidic ELISA chip

To test the aspiration performance of the hybrid microfluidic device, DI water was used as the working fluid and a gravimetric method was used to determine the aspiration volume and aspiration rate. In particular, the tip of the ELISA chip was immersed underneath a microplate well filled with water and a vacuum pressure (aspiration pressure from 0.5 to 3.0 psi) was applied to the RoMI interconnect of the device; the aspiration duration was precisely controlled with a solenoid valve, and the weight of the device before and after the aspiration process was measured with a high-precision balance (Mettler Toledo AB54-S/FACT). In such a way, the volume aspirated was determined, and the averaged aspiration rate was calculated by dividing the aspiration volume to the aspiration duration. It is worth noting that due to the hydrophilicity of the chip and capillarity of the liquid, a small amount of liquid (measured as 1.1 μL) remained at the tip of the chip; such remained volume of liquid was deducted in the calculation to increase the accuracy of characterization.

In the optimization of washing cycles, enzymatic reaction, and enrichment flow and cycles, we adopted the same concentration and volume ratios of the samples and reagents as those utilized in our previous study.[14] In the study of washing cycles, both membranes with or without the immobilized antibodies were prepared for different washing cycles, the enrichment flow was set at 2 psi and the enrichment cycle was 6. In the test of enzymatic reaction duration, the enrichment flow was set at 2 psi, the enrichment cycle was 6, and the washing cycle was 2. In the test of the enrichment cycle, the pressure for enrichment flow was 2 psi, the washing cycle was 2, and the enzymatic reaction duration was 6 min. In the test of the pressure for enrichment flow, the enrichment cycle was kept at 2 for all the

various pressures under test, the washing cycle was 2, and the enzymatic reaction duration was 6 min. With an enrichment volume of 25 μL and enrichment pressure of 1 psi, the net enrichment duration was 61.6 s for one cycle at a pressure of 2 psi, the enrichment duration was 35.2 s for one cycle at a pressure of 3 psi; the enrichment duration was 24.4 s for one cycle.

Demonstration of the automated sample-to-answer ELISA workflow

A competitive ELISA assay was designed and conducted for the automated detection of chloramphenicol (CAP) in a spiked sample, as a demonstration of the developed Robotic ELISA system. The relevant testing reagents were preloaded in a standard 96-well microplate (Greiner Bio-One Inc.), and then the microplate was sealed and stored at 4°C in the dark. As shown in Fig. 2, such reagents included 30 μL of 0.5 μg/mL (1.0 μg/mL for optimizing washing cycles) HRP-CAP (Abcam, USA) (Well ②), two 100 μL PBS washing buffer solutions (Well ④ & ⑤) and 30 μL TMB solution (Abcam, USA) (Well ⑥). Before the assay, the reagent-loaded microplate was transferred to the fixed location of the microplate holder on the testing stage and then unsealed, following which a sample solution (30 μL or more) was added to the microplate (Well ①). Since the z-position deviation caused by the robot movement or chip manufacturing was about 200 μm, an extra volume of 10 μL was added to the wells to ensure the effective contact of the tip of the ELISA chip with the liquid in the microplate wells. Such additional volume could be reduced by replacing the current microplates with wells that have smaller sizes.

In total, the sample solution and the relevant reagents occupied 6 wells. As shown in Fig. 2, the entire competitive ELISA protocol includes six steps: 1) aspirating 15 μL sample solution from Well ①; 2) aspirating 15 μL HRP-CAP solution from Well ②; 3) mixing the sample and the HRP-CAP solution in Well ③ to induce a competitive reaction with the immobilized antibodies on the membrane, by pneumatically driving the mixture solution to flow through the membrane back-and-forth, and then withdrawing the mixture to the same well after the reaction; 4) aspirating and withdrawing washing solution (36 μL PBS buffer) to the membrane to wash and remove unbound proteins, in Well ④ & ⑤ sequentially, and then air-drying the membrane under a high air pressure of 4 psi for 30 s; 5) aspirating 10 μL TMB solution from Well ⑥ to induce the enzymatic reaction; 6) recognizing the membrane and recording the grayscale values for 10 min every 2 min. The sample size was three for all experiments.

RESULTS AND DISCUSSION

Characterization of the aspiration process

As shown in Fig. 3a, the aspiration rates were determined under various pressure levels in the microfluidic devices with and without an incorporated nanofibrous membrane. For the devices without a nanofibrous membrane, the aspiration rate raised nearly linearly to the increment of the applied pressure, with a high correlation coefficient $R^2 = 0.999$. Specifically, the aspiration rate was 0.19 μL/s at 0.5 psi, and it increased to 1.01 μL/s when the pressure level was elevated to 3.0 psi. These results were consistent with the prediction from the hydraulic Ohm's law.[17] Accordingly, the averaged flow resistance of

the device could be computed, which was 20285 Pa·s/μL. On the other hand, the theoretical flow resistance could be calculated according to the analytical Poiseuille's equation under the laminar flow condition, for comparison.[20] As described in detail in ESI, the overall flow resistance was calculated approximately at 21677 Pa·s/μL, by considering resistances from the connecting serpentine microchannels, the detection chamber, and the liquid buffer chamber, of which the latter two were negligible. Though the theoretically determined flow resistance slightly deviated from (6.9%) the experimentally determined counterpart, it could offer a highly accurate approximation, which might be mainly altered by the dimensional (width and height) inaccuracies resulting from the microfabrication process. These results enabled that the aspiration rate could be conveniently adjusted by controlling the pressure applied.

Furthermore, we studied the control of aspiration volume by adjusting the pulse duration, as shown in Fig. 3b. At a fixed pressure of 1 psi, the aspirated volume was measured linearly proportional to the pulse duration, with a correlation coefficient of 0.9986. In particular, the aspiration volume was 7.6 μL at an applied duration of 15 s, and it was increased to 35.0 μL when the duration was extended to 90 s. Similarly, at a higher aspiration pressure of 2 psi, the aspirated volume was still found proportional to the aspiration duration with a correlation coefficient of 0.9983. The measured volume was 7.1 μL for 7.5 s of aspiration, and it was increased to 31.4 μL when the aspiration was extended to 45 s. In addition, at the same duration of 45 s, the aspiration volume was 18.4 μL for the aspiration pressure of 1 psi, while it was 31.4 μL for the pressure of 2 psi, approximately twice that of the 1 psi condition, as expected. These results confirm that the aspiration rate was approximately constant at the fixed pressure, and the aspiration volume can be conveniently adjusted by varying the duration of aspiration. We further determined the accuracy of the duration-adjusted aspiration volume, as shown in Fig. 3c. First, the required duration of aspiration for a specific desired volume was deducted from the fitting curve in Fig. 3b, which was 12.2 s for 10 μL, 19.9 s for 15 μL, 27.5 s for 20 μL, 35.2 s for 25 μL, and 42.9 s for 30 μL, respectively. Next, the actual aspirated volumes were measured, and they were 10.53 μL, 14.97 μL, 20.00 μL, 24.77 μL, 29.20 μL, respectively, under the aforementioned conditions. Therefore the accuracies for the desired volumes were calculated as 5.33%, 0.22%, 0.00%, 0.93%, and 2.67%, which consistently outperformed that of the commercial pipettes (with a claimed accuracy of 5%).[21]

Optimization of washing, enzymatic reaction and antigen enrichment

In this part, we intended to optimize the key parameters in the Robotic ELISA workflow, such as finding the optimal washing cycles, the optimal duration of the enzymatic reaction, and the optimal pressure and cycles for antigen enrichment, to achieve a rapid yet reliable sample-to-answer scheme.[14]

First, we investigated and determined the essential number of washing cycles for colorimetric readouts. One important criterion was that HRP-CAP unbound to the antibodies (on the membrane) should be completely washed away to avoid interferences with the TMB-associated colorimetric reaction. Both membranes with or without the immobilized antibodies were prepared, and they were subsequently reacted with HRP-CAP, followed by

washing with PBS buffers for different washing cycles; finally, the colorimetric reagent of TMB substrate was added and the corresponding time-evolved colorimetric results were illustrated in Fig. 4a. As can be seen, for the control membrane without immobilized antibodies, its color turned from white to blue rapidly within 2 min without the washing step. With washing once, however, a small margin on the edge of the membrane turned blue after 10 min, indicating that the majority of the HRP-CAP had been washed away. As we further increased the washing cycles to 2 and 3, as shown in the third and fourth rows, the color of the membrane did not change, indicating that the washing cycles were adequate. We further confirmed these conclusions by designing a positive control test. A membrane with immobilized antibodies was prepared and reacted with HRP-CAP, and it was then washed twice and reacted with TMB substrates. The colorimetric readouts are shown in the last row of Fig. 4a. As can be seen, the color of the membrane turned blue after 2 min of the enzymatic reaction. Overall, these results confirmed that the optimal washing cycle was 2 and therefore 2-cycle washes were used in all of the following experiments.

Next, we investigated the effects of the duration of enzymatic reaction on the colorimetric results, aiming to find the minimum incubation duration for reliable detection. Specifically, to quantify the color change of the nanofibrous membrane, the grayscale values (intensity) of the captured photos were extracted.[18,19] In particular, the average intensity value of each time-evolved photo was determined and the difference between the intensity value (at 2, 4, 6, 8 and 10 min) and the intensity value at the initial condition (0 min) was computed as Relative Intensity (RI). Next, the RI difference (ΔRI) between the readouts from a spiked solution (1 ng/mL CAP) and a negative control (PBS buffer) was calculated and used as an indicator for the sensitivity of the detection: a larger ΔRI meant greater sensitivity. As shown in Fig. 4b, for the negative control, ΔRI was 10.0 at 2 min, and it increased to 18.8 at 6 min and stayed almost still thereafter. Therefore, 6 min was considered the optimal duration for the enzymatic reaction and it was used in all of the subsequent experiments.

After that, we studied the enrichment conditions for the efficient Ag-Ab binding, including the enrichment cycle and the enrichment pressure, as summarized in Figs. 4c-d. Again, the control group of the PBS solution (negative) and the sample containing 1 ng/mL CAP (positive) were used to compare the colorimetric readouts. As shown in Fig. 4c, the ΔRI value was 7.5 without the enrichment cycle, and it increased to 16.7 after 2 cycles, 17.3 after 4 cycles and 18.8 after 6 cycles. As can be seen, the increase in the enrichment cycle had marginal effects on distinguishing the CAP-contained sample from the negative control. Consequently, 2-cycle enrichment was chosen as the optimal enrichment condition, which took approximately 200 s in total (1/3 that of the 6-cycle enrichment), to reduce the overall duration for the Robotic ELISA workflow. As can be seen, ΔRI for the 2-cycle enrichment was only less than 15% lower than that of the 6-cycle test. Though the sensitivity of detection was marginally compromised, the developed Robotic ELISA system was still capable of achieving a highly sensitive detection of our targeted analyte (CAP) in a short duration of mixing (within 2 cycles of enrichment).

Lastly, the effects of the enrichment pressure were also studied. As illustrated in Fig. 4d, the ΔRI value was 7.5 without the enrichment, and it increased to 19.0 at a pressure of 1 psi (with the flow rate of 0.41 μL/s); the ΔRI value decreased to 16.7 as the pressure increased

to 2 psi (with the flow rate of 0.69 μL/s), and it dropped to 8.0 as we further increased the pressure to 3 psi (with the flow rate of 1.02 μL/s). Since higher enrichment pressure generated faster flow, the flow might be too rapid , resulting in a short duration for the Ag-Ab binding.[5] Although the ΔRI for the 2-psi enrichment was 11% lower than that of the 1-psi enrichment, the enrichment duration at 2 psi was half that of the enrichment duration at 1 psi. Therefore, to minimize the overall duration of the Robotic ELISA workflow, 2 psi was chosen as the optimal pressure for the enrichment flow.

Demonstration of the fully automated ELISA operations

As investigated in the previous Section, the optimized washing and reaction steps were applied, in which both the washing and enrichment cycles were 2 with the enzymatic reaction duration of 6 min under the enrichment pressure of 2 psi. To demonstrate the fully automated human-free sample-to-answer workflow, the Robotic ELISA platform was programmed for the detection of CAP concentration ranging from 0 to 2 ng/mL (or 0 to 6.2 nM) in a spiked sample, which included the automated metering, mixing, washing and colorimetric readouts.

Fig. 5a illustrates the time-evolution of the color change of the nanofibrous membrane during the enzymatic reaction, under six different CAP concentrations from 0 to 2 ng/mL. For each CAP concentration, a group of six photos was captured, which included the initial condition of the membrane and its subsequent conditions every 2 min thereafter. As can be seen, for a low CAP concentration at 0 ng/mL, the color of the membrane was initially light grey; the color started to change to blue after 2 min, and it rapidly turned into blue within 4 min and stayed unchanged afterwards (a blue color means CAP is not present). On the other hand, for the case of a high CAP concentration at 2 ng/mL, the initial color was the same with gradual transition to blue; however, the color change of the membrane was rather slow, and it stayed in the grey-blue mix even after 10 min of reaction. Such results confirmed the fact that the CAP from the sample competed with that in the HRP-CAP solution and therefore inhibited the binding of the HRP-CAP to the immobilized antibodies on the membrane, altering the colorimetric readouts.

To further quantify the colorimetric results and determine the sensitivity and limit of detection (LOD), three devices were tested for each CAP concentration, and Fig. 5b showed the average results of the RI values. The linear range was found to be between 0 to 1 ng/mL (R^2 =0.973).[14] As can be seen, the RI value was 29.3 ± 0.58 for the CAP concentration of 0 ng/mL and it decreased to 12.7 ± 1.53 at 1 ng/mL. The absolute value of the sensitivity was therefore determined as 16.6/(ng/mL). Since the standard deviation of the negative control group was 0.58, the LOD was set at 0.1 ng/mL.[22] It is worth noting that the LOD achieved by the Robotic ELISA system outperforms that conducted by manually operated nanofibrous membrane-based ELISA using the same colorimetric readout, which is 0.3 ng/mL.[14] Furthermore, the LOD is comparable to the conventional microtiter plate reader-based ELISA detection.[23] As a conclusion, these results demonstrate that the Robotic ELISA is comparable to competitive ELISA,with a low detection limit of 0.1 ng/mL.

CONCLUSION

In summary, we have developed a fully automated platform, known as Robotic ELISA, seamlessly incorporating a robotic-microfluidic interface (RoMI) and a nanofibrous membrane-embedded hybrid microfluidic chip, for the human-free sample-to-answer workflow of the conventional ELISA tests. The Robotic ELISA allows automated multiplex operations such as high-precision pipetting, back-and-forth mixing and enrichment, washing and vision-unit enabled colorimetric readout. Compared to the existing ELISA automation solutions, the Robotic ELISA offers several distinct advantages: 1) fully automated ELISA detection; 2) short overall operation time (less than 20 min) from sample to answer; 3) high sensitivity and low limit of detection (0.1 ng/mL) for CAP; and 4) low sample consumption (15 μL). Benefiting from its modular design and automated operations, the robotic ELISA platform becomes a promising candidate for a broad range of detections in resource-limited settings or high-risk environments, where human involvement needs to be minimized, while the testing timeliness, consistency and sensitivity are all desired.

Supplementary Material

Refer to Web version on PubMed Central for supplementary material.

ACKNOWLEDGMENT

This research work was partially supported by the NIEHS UC Davis Superfund Project (5P42ES004699-30), USDA-NIFA (grant no. 2018-67017-28116/project accession no. 1015597], Guangdong Program (2016ZT06D631), Shenzhen Fundamental Research Program (JCYJ 20170413164102261), and Shenzhen Engineering Laboratory of Single-molecule Detection and Instrument Development (Grant No. XMHT20190204002). The authors would like to acknowledge Ka Deng and Gavin Huang for their assistance in Python programming. Any opinions, findings, conclusions, or recommendations expressed in this publication are those of the author(s) and do not necessarily reflect the view of the U.S. Department of Agriculture or NIH.

REFERENCES

(1). Vinet L; Zhedanov AA“missing” Family of Classical Orthogonal Polynomials; 2011; Vol. 44.

(2). Carter LJ; Garner LV; Smoot JW; Li Y; Zhou Q; Saveson CJ; Sasso JM; Gregg AC; Soares DJ; Beskid TR; Jervey SR; Liu CAssay Techniques and Test Development for COVID-19 Diagnosis. ACS Cent. Sci2020, 6 (5), 591–605. [PubMed: 32382657]

(3). Lequin RMEnzyme Immunoassay (EIA)/Enzyme-Linked Immunosorbent Assay (ELISA). Clin. Chem2005, 51 (12), 2415–2418. [PubMed: 16179424]

(4). Hosseini S; Vázquez-Villegas P; Rito-Palomares M; Martinez-Chapa SOEnzyme-Linked Immunosorbent Assay (ELISA): From A to Z; 2018.

(5). Sanjay ST; Li M; Zhou W; Li X; Li XJA Reusable PMMA/Paper Hybrid Plug-and-Play Microfluidic Device for an Ultrasensitive Immunoassay with a Wide Dynamic Range. Microsystems Nanoeng. 2020, 6 (1).

(6). Khodayari Bavil A; Kim JA Capillary Flow-Driven Microfluidic System for Microparticle-Labeled Immunoassays. Analyst2018, 143 (14), 3335–3342. [PubMed: 29878004]

(7). Yang M; Sun S; Kostov Y; Rasooly AAn Automated Point-of-Care System for Immunodetection of Staphylococcal Enterotoxin B. Anal. Biochem2011, 416 (1), 74–81. [PubMed: 21640067]

(8). Lee BS; Lee JN; Park JM; Lee JG; Kim S; Cho YK; Ko CA Fully Automated Immunoassay from Whole Blood on a Disc. Lab Chip2009, 9 (11), 1548–1555. [PubMed: 19458861]

(9). Zheng C; Wang J; Pang Y; Wang J; Li W; Ge Z; Huang YHigh-Throughput Immunoassay through in-Channel Microfluidic Patterning. Lab Chip2012, 12 (14), 2487–2490. [PubMed: 22549364]

(10). Apilux A; Ukita Y; Chikae M; Chailapakul O; Takamura YDevelopment of Automated Paper-Based Devices for Sequential Multistep Sandwich Enzyme-Linked Immunosorbent Assays Using Inkjet Printing. Lab Chip2013, 13 (1), 126–135. [PubMed: 23165591]

(11). Fu H; Song P; Wu Q; Zhao C; Pan P; Li X; Li-Jessen NYK; Liu XA Paper-Based Microfluidic Platform with Shape-Memory-Polymer-Actuated Fluid Valves for Automated Multi-Step Immunoassays. Microsystems Nanoeng. 2019.

(12). Kim J; Jensen EC; Megens M; Boser B; Mathies RAIntegrated Microfluidic Bioprocessor for Solid Phase Capture Immunoassays. Lab Chip2011, 11 (18), 3106–3112. [PubMed: 21804972]

(13). Li F; You M; Li S; Hu J; Liu C; Gong Y; Yang H; Xu FPaper-Based Point-of-Care Immunoassays: Recent Advances and Emerging Trends. Biotechnology Advances. 2020.

(14). Zhao C; Si Y; Pan B; Taha AY; Pan T; Sun GDesign and Fabrication of a Highly Sensitive and Naked-Eye Distinguishable Colorimetric Biosensor for Chloramphenicol Detection by Using ELISA on Nanofibrous Membranes. Talanta2020, 217.

(15). Wang J; Deng K; Zhou C; Fang Z; Meyer C; Deshpande KUA; Li Z; Mi X; Luo Q; Hammock BD; Tan C; Chen Y; Pan TMicrofluidic Cap-To-Dispense (MCD): A Universal Microfluidic-Robotic Interface for Automated Pipette-Free High-Precision Liquid Handling. Lab Chip2019, 19 (20), 3405–3415. [PubMed: 31501848]

(16). de Gennes P-G; Brochard-Wyart F; Quéré DCapillarity and Wetting Phenomena; 2004.

(17). Oh KW; Lee K; Ahn B; Furlani EPDesign of Pressure-Driven Microfluidic Networks Using Electric Circuit Analogy. Lab on a Chip. 2012, pp 515–545. [PubMed: 22179505]

(18). Luo X; Xia J; Jiang X; Yang M; Liu SCellulose-Based Strips Designed Based on a Sensitive Enzyme Colorimetric Assay for the Low Concentration of Glucose Detection. Anal. Chem2019, 91 (24), 15461–15468. [PubMed: 31710204]

(19). Liu W; Guo Y; Zhao M; Li H; Zhang ZRing-Oven Washing Technique Integrated Paper-Based Immunodevice for Sensitive Detection of Cancer Biomarker. Anal. Chem2015, 87 (15), 7951–7957. [PubMed: 26140306]

(20). Sutera SP; Skalak RThe History of Poiseuille's Law. Annu. Rev. Fluid Mech1993, 25 (1), 1–20.

(21). Fan J; Men Y; Hao Tseng K; Ding YY; Ding YY; Villarreal F; Tan C; Li B; Pan TDotette: Programmable, High-Precision, Plug-and-Play Droplet Pipetting. Biomicrofluidics2018, 12 (3).

(22). Long GL; Winefordner JDLimit of Detection: A Closer Look at the IUPAC Definition. Anal. Chem1983, 55 (7), 712A–724A.

(23). Wesongah JO; Murilla GA; Guantai AN; Elliot C; Fodey T; Cannavan AA Competitive Enzyme-Linked Immunosorbent Assay for Determination of Chloramphenicol. J. Vet. Pharmacol. Ther2007, 30 (1), 68–73. [PubMed: 17217404]

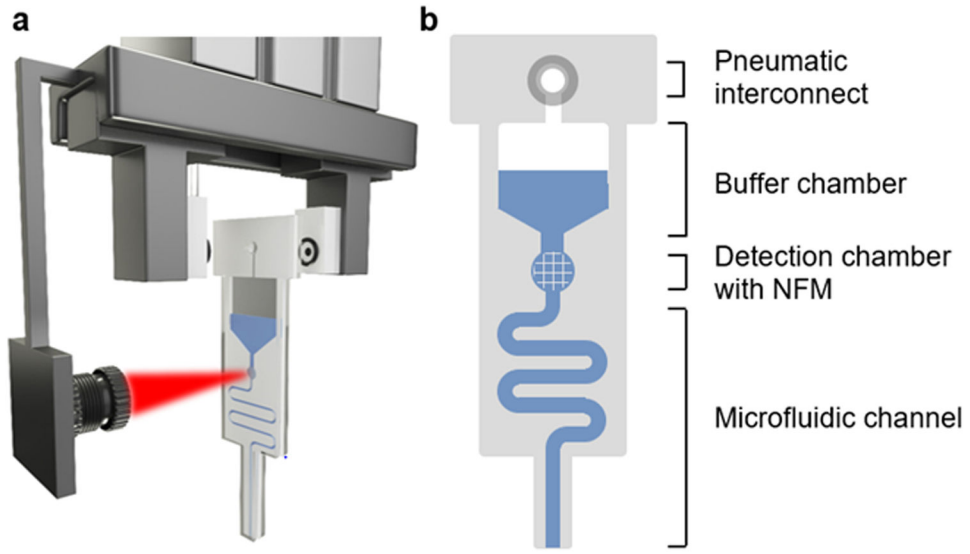

Figure 1.

Concept of the Robotic ELISA system. a) Illustration of the Robotic ELISA platform; b) illustration of the nanofibrous membrane (NFM)-contained hybrid microfluidic chip.

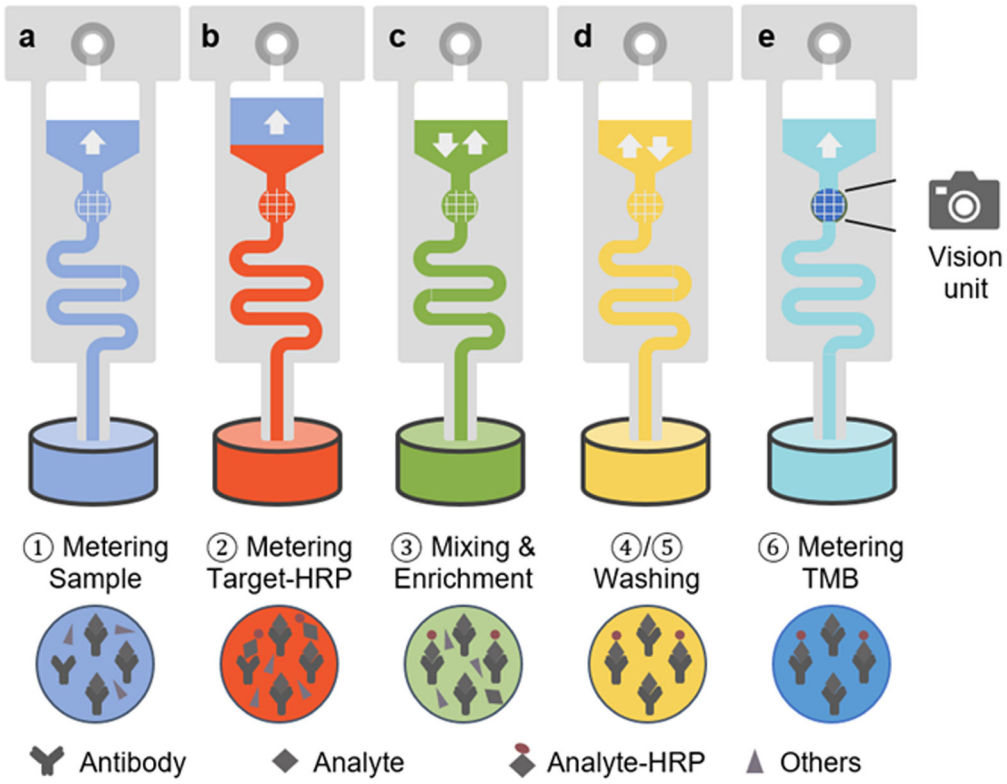

Figure 2.

Illustration of the Robotic ELISA operations, including a-b) high-precision metering, c) mixing and enrichment, d) washing, e) enzymatic reaction, and robotic vision unit enabled imaging and detection.

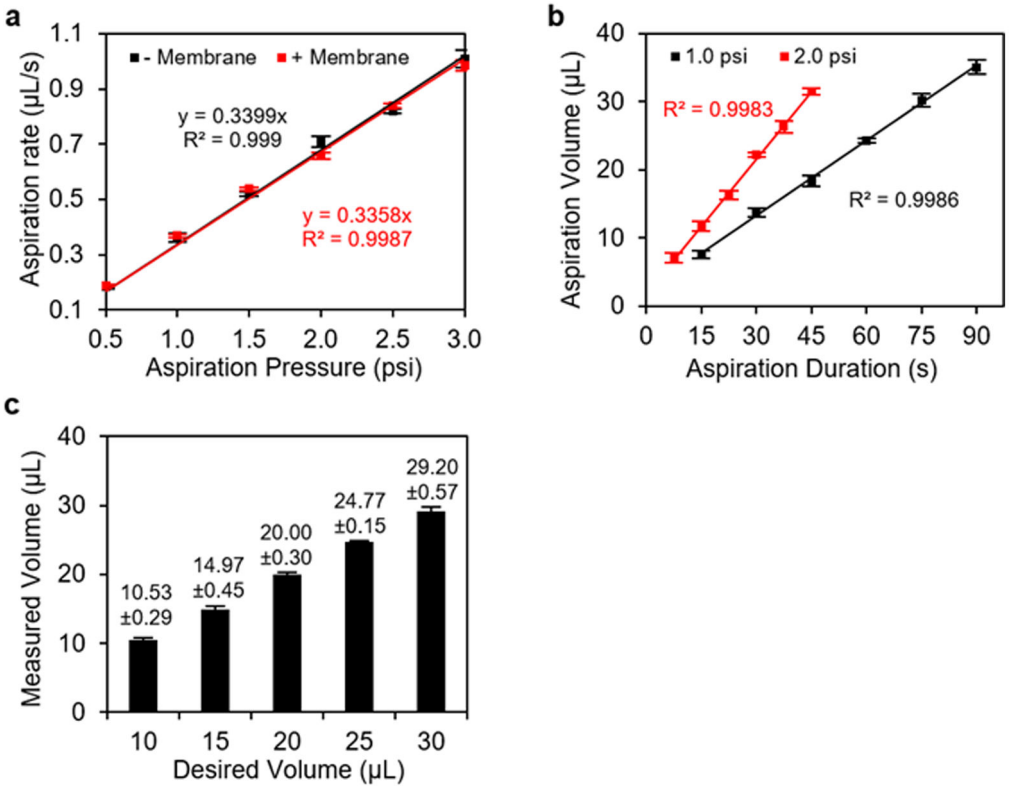

Figure 3.

a) The aspiration rates of the hybrid microfluidic chip under various pressure levels from 0.5 to 3.0 psi, with or without the nanofibrous membrane; b) the aspiration volume under various pulse durations from 10 to 90 s, given the pressure applied at 1 and 2 psi, respectively; and c) the measured accuracy of the aspiration volume for a desired volume from 10 to 30 µL.

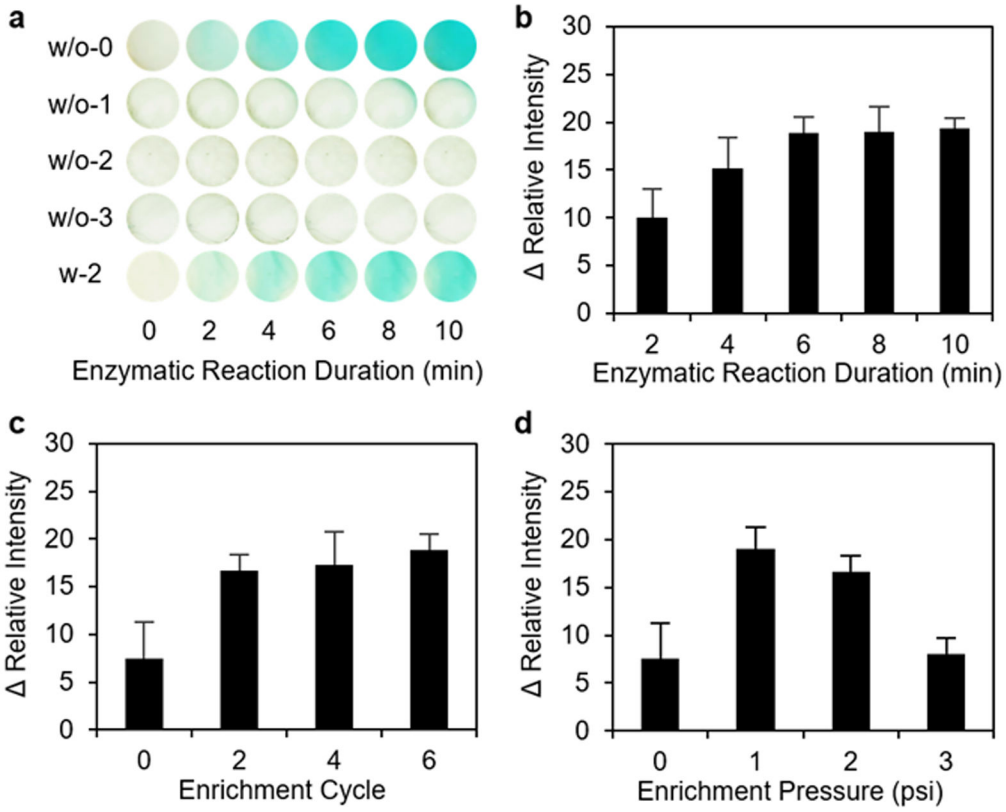

Fig. 4.

Optimization of washing, enzymatic reaction, and antigen enrichment conditions. a) Images of the nanofibrous membrane with (w/) or without (w/o) the immobilized antibodies after adding the colorimetric reagent of TMB substrate to induce the enzymatic reaction under various washing cycles from 0 to 3. Comparison of the difference of the relative intensity value (i.e., ΔRI) under various b) enzymatic reaction durations from 2 to 10 min, c) enrichment cycles from 0 to 6, and d) pressure for enrichment flow from 0 to 3 psi ("0" means "no enrichment") for a negative control (PBS buffer) and a sample containing 1 ng/mL CAP. Note that the error bar indicates the measurement deviation between three different devices.

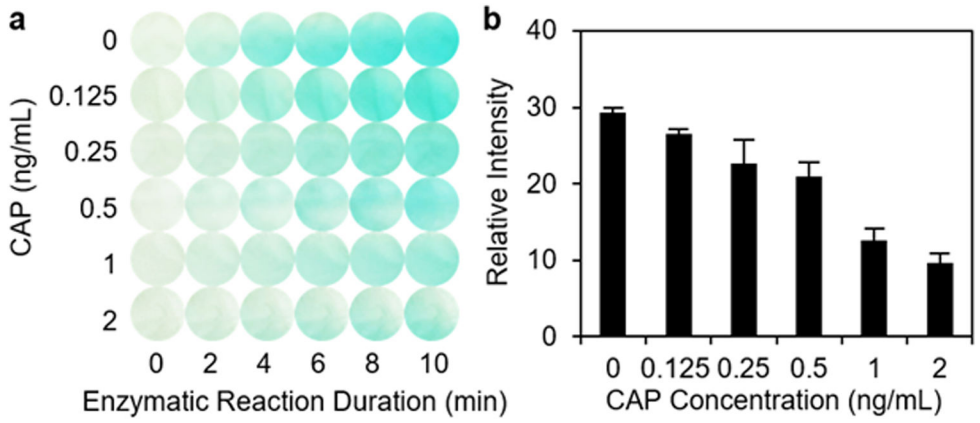

Fig. 5.

a) Time-evolved optical images of the membrane from 0 to 10 min under various concentrations of CAP from 0 to 2 ng/mL, and b) Relative Intensity value between the colorimetric readouts at 6 min and the initial condition (0 min) under various concentrations of CAP from 0 to 2 ng/mL. Note that the error bar indicates the measurement deviation between three different devices.

Table 1

Comparisons of current automation schemes of ELISA

Device Types		Liquid Handling	Detection	LOD (ng/mL)	Time (min)	Vol-ume (μL)	Automa-tion	Ref.
Microtiter plate	Conventional 96 well plate	Robotic pipettor, plate washer	Spectrophotometer	1.6-6.25	Over-night	50-100	Fully	5
Polymeric chip	Passive microfluidics	Capillarity enabled automated liquid transfer	Optical microscope	0.1	<10	~1	Partially	6
	Off-the-chip valves and pumps	Syringe pumps and valves	CCD camera/scanner	0.1	45+	20	Partially	7
	Centrifugal discs	Centrifuge and laser irradiated ferrowax microvalves	Optical absorbance detector	0.51	30	50	Fully	8
	In-channel microfluidic patterning	Embedded pneumatic valves	Fluorescence microscope	0.01	60	<1	Partially	9
Paper-based chip	Patterned nitrocellulose (NC) membrane	Capillarity enabled automated liquid transfer	Digital camera	0.81	15	100	Partially	10
	Chromatography paper with patterned valves	Thermally actuated valves	Light transmittance detector	4	55	3	Partially	11
Hybrid chip	PMMA/paper	Syringe pump	Scanner/phone camera	0.2	70	25	Partially	5
	PMMA/NFM	Pressure controller, solenoid valve, and robotic arm	Digital camera	0.1	20	15	Fully	This work